

# Low-cost 3D-Printable Docking System for Controlling Aerial Robotic Manipulators in Outdoor Industrial Applications

Pablo Ramon Soria<sup>1</sup>, B.C. Arrue<sup>1</sup>, Anibal Ollero<sup>1</sup>

**Abstract**—This paper proposes a novel design of a docking system for Unmanned Aerial Vehicles (UAVs) which provides measurements of the position of the robot at high frequency. These measurements are used for controlling the aerial robot, enabling it to hover while it performs any kind of manipulation task in GPS denied industrial environments without causing the UAV to drift and putting into risk the platform and its environment. The novel tool is designed as end-effector of an arm preventing the aerial manipulator to collide while operating. A cascade controller is proposed to close the position loop.

The prototype system is 3D printed in ABS. The paper presents outdoor experimental results. The accuracy of the system is evaluated against GPS, a state of art visual algorithm and a laser total station as a ground truth. The measurements obtained from the docking tool exceed a frequency of 1000 Hz which overtakes common localization algorithms.

## I. INTRODUCTION

In recent years, the interest in aerial robots has increased. Their capability of moving freely in the space allow them to work in several situations. Montambault et al. in [1] exposes a review of multiple civil and industrial applications with UAVs. Particularly, there is an increment of applications in inspection and maintenance tasks in factories and power stations. Their ability to access to high altitude locations, which can be dangerous for human operators, have make them very popular in these applications. However, their usage is usually only perceptive.

Large-scale industrial facilities, such as factories or energy power stations, require intensive and costly labors of inspection and maintenance. Innovative solutions use robots to automate such tasks in-situ. Authors in [2] use a combination of line detection and feature detection for locating wind turbines for inspection purposes. Addabbo et al. in [3] use thermal images for locating and inspecting solar panels in photo-voltaic plants.

However, an extra effort needs to be made to allow robots to perform maintenance or repair tasks. In order to enable UAVs to interact with the industrial facilities, recent researches provide them with manipulators. Orsag et al. in [4] point out the key challenges for controlling UAVs with embedded manipulators. Authors in [5] implement an impedance control to improve the actuation of the robot against the external disturbances produced by the arm. They applied the control algorithm in simulations. In [6], authors proposes a multi-layered control that takes into account the

movements of the built-in arm for improving the control of the UAV. Another approach can be found in [7], in which authors describe an adaptive sliding mode controller.

Authors in [8] developed an aerial robot equipped with a pair of manipulators for actuating valves. They study the forces applied on the robot resulting from turning the valve and show experiments in an indoor controlled environment. Another dual-arm system for UAVs is developed in [9]. In this paper, authors focus on the torque effects on the UAV due to the movement of the pair of arms while hovering. Typically, built-in arms are articulated robots, work in [10] uses a parallel manipulator at the bottom of the UAV.

Authors in [11] analyze the forces exerted on an UAV in contact with an stiff environment, such as wall, in simulations. With a similar purpose, authors in [12] designed a device that measures forces in contact with stiff surfaces. They use that information to control the position of the aerial robot and the force exerted by it.

Nevertheless, most studies perform the experiments at indoor test-beds using OPTITRACK or VICON systems. These localization systems provide accurate and fast measurements of the positions of the robots. They are useful for validating algorithms but are not realistic assumptions for outdoors applications.

Several researches about positioning robots are based on vision sensors such as color cameras, RGB-D cameras and LiDARs. In these cases, the location of the robot is tackled following a SLAM procedure. Algorithms such as ORB-SLAM [13], RTAB-MAP [14], LOAM [15] and many others have been proved to be good general purpose solutions. Nonetheless, they rely on visual landmarks and high cost computational operations that need to be performed in the on-board computers. Additionally, the algorithms can get lost due to occlusions or lack of landmarks.

The main contribution of the article is the design of a novel tool, from now on docking tool, that allows aerial robots to remain flying close to a target position in outdoor environments, without needing any other external device. This device has the advantage of providing a high rate of measurements of the robot position with a few computational cost, thus the rest of power resources of the computer can be used for other tasks or even carrying a smaller computer without compromising the payload of the platform.

The remainder of the paper is organized as follows. Section II presents the model of the proposed tool. Section III presents the control system. Later, in Section IV, experimental results are shown to support the design. Conclusions and future work are presented in Section V

<sup>1</sup>Group of Robotics, Vision and Control, University of Seville, Av. de los Descubrimientos, Seville 41092, Spain, {prs,barrue,aollero}@us.es

## II. LOW-COST DOCKING SYSTEM

This section describes the hardware design of the novel tool. The development of tools for aerial robots is usually more constrained than in ground systems due to the payload limitations and stability issues. In this work, the following assumptions are adopted:

- Perturbations produced by wind are relatively small.
- The UAV has a low-level controller which input is a desired speed in Cartesian coordinates and it outputs motors speed.

To accomplish the first assumption the system has been tested in low wind conditions. For the second assumption, the robot is equipped with a PIXHAWK [16] autopilot that uses px4 software [17].

The aerial robot has two built-in arms, each of them with a different tool. The right arm is provided with a gripper to perform different manipulation tasks. The docking tool is attached to the left one. This tool provides the position of the UAV relative to its attachment base. These measurements are used for stabilizing it close to the manipulation space. Figure 1 shows the aerial robot with all the tools.



(a)



(b)

(c)

Fig. 1. (a) dual arm aerial robot with gripper and docking tool. (b) and (c) show the quick release system for attaching different tools, i.e. the gripper or the docking tool.

### A. Arm model

Each arm is composed by three rotation joints and a general purpose end-tool socket with an extra rotation in the direction of the arm. The first rotation is in the Z axis and the two remaining rotations compose a two-link arm.

Hence, each arm has four degrees of freedom (DoF). The end-effector has a quick release system that makes it easy to replace any tool as shown in Figures 1b) and c). The arms are part of the open-source project *Hecatonquiros*<sup>1</sup> developed by

<sup>1</sup><https://github.com/vigus/hecatonquiros>

the Group of Robotics Vision and Control of the University of Seville. This project aims for a cheap and easy to use framework for aerial manipulation.

### B. Docking tool model

This section describes the model of the docking tool. It consists of a passive multi-link arm with sensors in the joints to measure the angles between the links.

The main criteria during the design of the tool was to minimize the total weight and the friction in the joints, reducing the torques exerted on the arm and subsequently on the UAV. In order to reduce the weight, the structural parts are designed thin and hollowed. The components are 3D printed using ABS, being lightweight and easier to replace. Furthermore, the production costs are lower than using aluminum or carbon fiber and the components do not need to be built, mechanized or post-processed.

The tool is not actuated, i.e. it does not need any motor, being lighter and getting rid of battery weight. Figure 2(a) shows the CAD model of the tool. Bearings have been placed in the joints to minimize the friction. These are made of acetal plastic which are ten times lighter than common metal bearings.

It is composed by five joints. The base joint (or  $\theta_0$ ) provides a rotation on the Z axis. The following two joints ( $\theta_1$  and  $\theta_2$ ) compose a two-link arm that gives to the robot free 3D movement on the work zone. Joint  $\theta_3$  are set to provide an extra degree of freedom allowing the robot to remain parallel to the floor, independently of the position of the two-link section. Finally, the last joint ( $\theta_4$ ) adds to the robot another DoF, to make it able to maintain the heading effortlessly.

The kinematic model is shown in equation 1

$$T_{UAV} = f(\theta_0, \theta_1, \theta_2, \theta_3, \theta_4) = T_0 \cdot T_1 \cdot T_2 \cdot T_3 \cdot T_4 \quad (1)$$

being,

$$T_0 = \begin{bmatrix} c\theta_0 & -s\theta_0 & 0 & 0 \\ s\theta_0 & c\theta_0 & 0 & 0 \\ 0 & 0 & 1 & l_0 \\ 0 & 0 & 0 & 1 \end{bmatrix} \quad (2)$$

$$T_i = \begin{bmatrix} 1 & 0 & 0 & l_i \\ 0 & c\theta_i & -s\theta_i & 0 \\ 0 & s\theta_i & c\theta_i & 0 \\ 0 & 0 & 0 & 1 \end{bmatrix} \quad \forall i = 1, 2, 3 \quad (3)$$

$$T_4 = \begin{bmatrix} c\theta_4 & 0 & s\theta_4 & 0 \\ 0 & 1 & 0 & l_4 \\ -s\theta_4 & 0 & c\theta_4 & 0 \\ 0 & 0 & 0 & 1 \end{bmatrix} \quad (4)$$

The docking tool system has 5 DoF for the drone's movement. An additional joint in the axis of latest bar has been considered too to provide free rotation related with roll of the UAV. However, this rotation is significantly small due

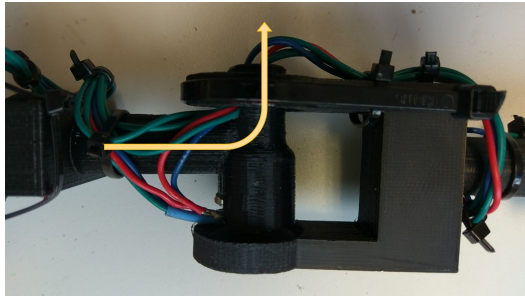


Fig. 2. a) shows the CAD model of docking tool with basement for attaching to pipes. b) shows a close picture of the wiring system.

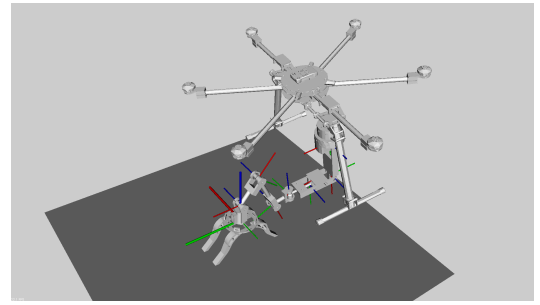
to the assumption of small perturbations. For this reason, the joint is not included in the design.

The joints of the tool are provided with potentiometers that are used for measuring the angles. The voltage signals from the potentiometers are measured by an electronic device connected to the on-board computer. Then, the signals are mapped to angles. Because the voltage in the resistances changes linearly, the mapping of variables is a linear map.

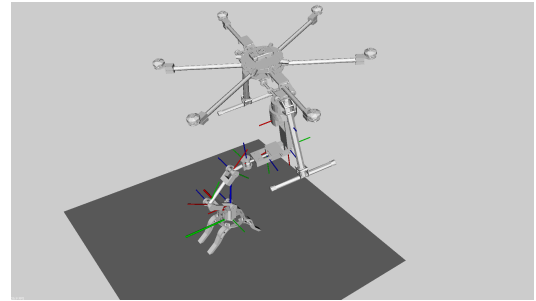
The sensors are wired using internal holes on the joints as shown in Figure 2(b). This minimize the forces exerted by the cables on the joints.

The angles measured from the potentiometers are used to estimate the current pose of the UAV. Together with the information of the arms, these measurements are used to close the loop of the control system described in section III. Figure 3 shows a 3D virtual visualization at different times of real experiments.

More detailed specifications of the docking tool compo-



(a)



(b)

Fig. 3. Online virtual visualization of the aerial platform with the docking tool during the experiments.

nents are summarized in Table I.

TABLE I  
SPECIFICATIONS OF THE LOW-COST DOCKING TOOL

Potentiometers resistance( $K\Omega$ )	20	
Potentiometers angle range(deg)	270	
Operating Voltage (V)	5	
Power consumption (W)	0.25	
Longitudes (m)	$l_0$	0.071
	$l_1$	0.105
	$l_2$	0.155
	$l_3$	0.07
	$l_4$	0.075
Total weight (g)	150	
Base material	Plastic ABS	

### III. CONTROL LOOP

A cascade control system is proposed for positioning the aerial robot. Figure 4 shows the controller structure. The inner loop corresponds to the internal controller provided by the px4 software. It consists of a Cartesian speed control that translates from a desired velocity to the corresponding actuation on the motors. The outer loop uses the position obtained by the docking tool to produce a target speed to control the robot.

The outer controller is a PID

$$u(t) = K_p e(t) + K_i \int_0^t e(t) dt + K_d \frac{de(t)}{dt} \quad (5)$$

tuned to provide quick responses to the perturbations on the UAV and to the drifts of the internal controller (generally

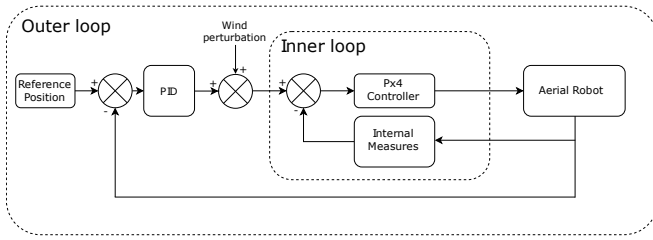


Fig. 4. Scheme of the cascade control system.

due to errors in the internal estimators of the px4 software: GPS errors, IMU drifts, etc.)

While the tool is docked, it throws measures of the relative position from its basement. The error that feeds the control loop is computed by the difference in position of the current position and a reference position. In order to smooth the state of the robot, the data obtained from the tool is filtered using an Extended Kalman Filter[18].

The PID was coded with an anti-windup system to avoid large oscillations due to the integral factor. Additionally, the output speeds are saturated to prevent abrupt control signals due to the derivative terms. Table II contains the values of the PID parameters. These values were roughly tuned from the experiments

TABLE II  
PID PARAMETERS

	$K_p$	$K_i$	$K_d$	Anti-windup	Signal saturation (m/s)
X	0.8	0.01	0.7	30	2
Y	0.8	0.01	0.7	30	2
Z	0.3	0.03	0.7	30	1

## IV. EXPERIMENTAL VALIDATION

This section presents the experiments performed to validate the tool.

### A. Experimental Setup

In addition to the components in Section II, the aerial robot needs other devices to perform the experiments. Figure 5 shows all system components. The arms are actuated using the PWM ports of an Arduino Mega ADK micro-controller. The potentiometers on the joints of the docking tool are connected to the analog inputs of the micro-controller too. The Arduino is connected to an on-board Intel NUC computer which is used as main computer. The lectures of the sensors are gathered on it, to produce the control signals that are sent to the autopilot (Pixhawk). The autopilot receives the target speed and controls the multi-rotor. Additionally, a power supply system is added to feed each of the devices at custom voltages.

A set of practical conclusions were obtained during the first stages of the development process:

- In order to increase the arms operation range and to prevent internal collisions a foldable landing gear was built-in.

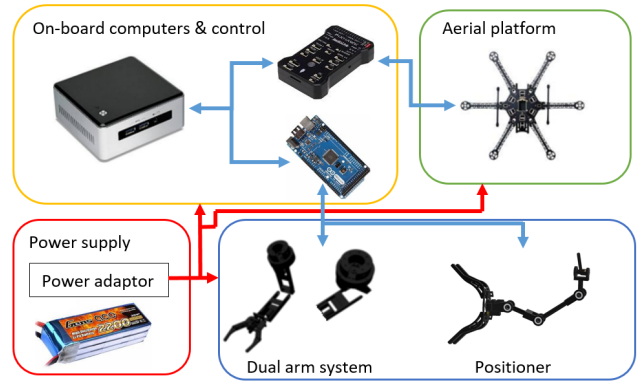


Fig. 5. Components of the autonomous docking system.

- It was observed that signals of potentiometers saturate before reaching the mechanical extremes. This reduces the tool workspace. Particularly, the mechanical range is  $170^\circ$  and the signal range is  $150^\circ$ . For this reason, it is good to keep the UAV in a position in which the joints are not in the limits.
- The docking tool joints are not actuated. During the experiments the tool hangs until it is docked. Particularly, the base joint can rotate. For this reason, that joint is locked with a microservo which unlocks the joint once the tool is placed.

### B. Test-bench and tool characterization

A static experiment has been carried out in a test-bench. The purpose is to measure two variables: the accuracy and the frequency of the measurements. The data provided by the docking tool is compared against a ground truth obtained by a *Leica Total Station MS50*<sup>2</sup> (or TS). It uses a laser that locates a *prism* within an error of 0.3 – 0.4 millimeters.

The docking tool is placed on a table and the *prism* is attached at the end of the positioning system as shown in Figure 6.

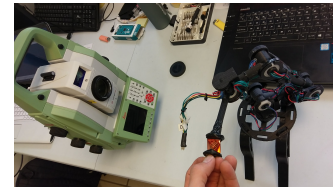


Fig. 6. Test-bench with laser system for measuring the accuracy of the docking tool.

Figure 7 shows the results in the test-bench. The end position of the tool is moved describing a cross in 3D, trying to perform the movements over each axis independently. Figure 7(a) shows the end-position of the tool, the solid line is the position measured by the docking tool and the dashed line is the position measured by the TS taken as ground truth; Figure 7(b) shows the difference between both measures. The

<sup>2</sup><https://leica-geosystems.com/products/total-stations>

mismatch in the Z axis, within time counts 2375 and 2675, corresponds to the fact that the values of the potentiometers saturate when going down. The joints exceed the allowed range which leads to bad angle measurements. Similar effects can be seen at the limits of the movements in the X and Y axis but in these cases the effect is slightly noticeable. Figure ?? shows a representation of the 3D movement performed during the experiment.

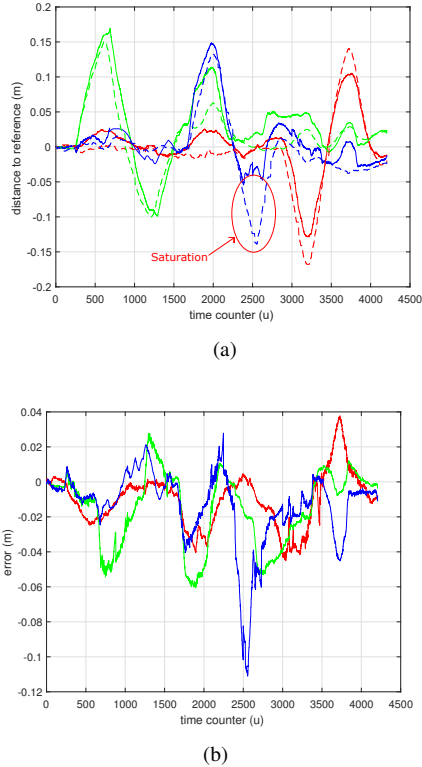


Fig. 7. 7(a) shows the X, Y, Z components of the trajectory of the end-effector during the experiment in the test-bench measured by the docking tool and the laser system (X: red; Y: green; Z: blue). 7(b) shows the relative error between the measurements. The relative error has been zoomed for the clearness of the figure.

### C. GPS positioning characterization

An outdoor first experiment has been executed using the GPS as position reference for the control loop. This experiment is shown to characterize the magnitude of typical errors using this common positioning device and to compare with our positioning system. The real position of the robot is measured with the Total Station. Figure 8 shows the error in the position of the UAV according to a fixed set point measured with the Total Station.

In this experiment, it can be observed that the errors can be large in some situations. Moreover, these experiments were performed outdoors in a clear day, there could be worst conditions where the GPS could be denied or noisy, inducing larger errors and putting the platform and the environment in danger. This inaccuracy exceeds the workspace of the arms, making difficult any kind of inspection or manipulation task in the target zone.

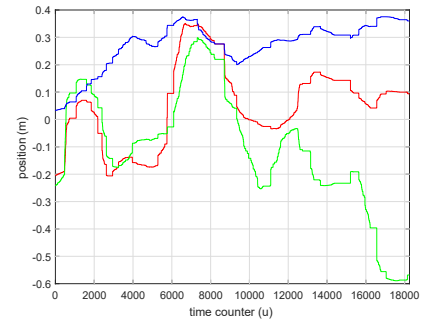


Fig. 8. Test experiment for characterizing the error using GPS and the internal estimator of the UAV (X: red; Y: green; Z: blue).

### D. Docking and autonomous control

During the experiment<sup>3</sup>, the UAV takes off, moves to the target position in order to attach the docking tool. Then, it starts measuring the relative position of the robot and performs the autonomous control. The position of the UAV is also acquired using the TS as ground truth. Figure 9 shows snapshots of different experiments of the robot docked to a pipe.



Fig. 9. Snapshots of robot docked to a pipe during different experiments. The joints of the docking tool, passively, adapt to the UAV position, which can vary due to external perturbations.

Additionally, a camera has been attached to the docking tool to compare the results with a monocular vision system (ORB\_SLAM2[13]). In Figure 10 the data recorded during an experiment using the docking system can be observed. Figures 10(a), 10(b) and 10(c) show the difference between the current position and the reference position measured by the different localization systems. The solid line represents the difference in position by the docking tool. The dashed line the one measured by the total station and the solid line with dots using the vision algorithm.

Figure 10(d), shows the control signals produced by the PID generated by the outer loop of the cascade controller

<sup>3</sup>[https://youtu.be/Vk9G71b\\_r6I](https://youtu.be/Vk9G71b_r6I)

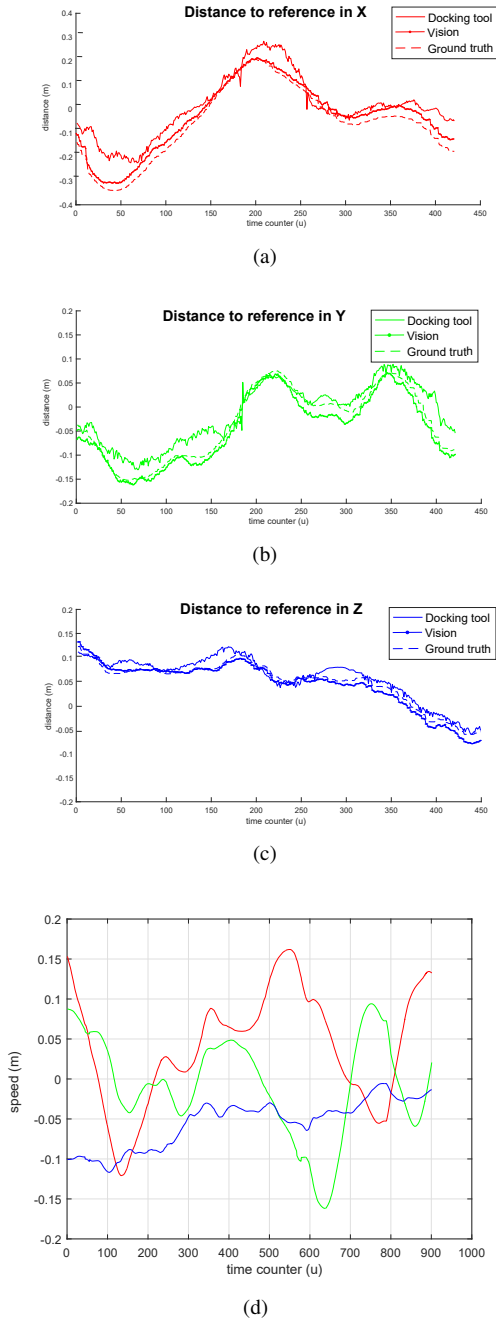


Fig. 10. 10(a), 10(b) and 10(c) compare the errors between current drone's position and a reference position measured from the docking tool (solid line) and the TS (dashed line) and the vision system (solid line with dots) in the three axis. 10(d) shows the speed control generated for the outer loop of the cascade controller

from the error in position obtained by the docking tool.

Table III compares the errors and deviations of the different localization systems studied against the docking tool during the experiments at each axis. It is evident, that just relying on GPS is unsafe for the platform. It can be observed, that both the visual algorithm and the docking tool provides similar measures, being the ones of the docking tool slightly less accurate. However, the visual localization algorithm consumes a lot of computer's resources and it

gives the location of the robot up to 25 Hz. Conversely, the measurements obtained from the docking system achieve a frequency of 1200 Hz which overtakes the vision speed. Moreover, the computer vision approach depends strongly on the lighting conditions.

TABLE III

ERRORS AND STANDARD DEVIATIONS DURING THE TEST EXPERIMENTS.

	GPS		Vision		Docking Tool	
	$\mu$	$\sigma$	$\mu$	$\sigma$	$\mu$	$\sigma$
x (m)	0.164	0.079	0.022	0.027	0.034	0.032
y (m)	0.153	0.123	0.012	0.032	0.036	0.028
z (m)	0.179	0.085	0.023	0.026	0.040	0.039
avg. speed (Hz)	10		25		1200	

## V. CONCLUSIONS AND FUTURE WORK

It has been proposed a low cost and low weight docking system for a dual arm aerial manipulator in flight. It has been shown that the tool provides high-rate and accurate measurements of the aerial robot relative position from a target zone. This tool allows the robot to operate even in GPS denied conditions. Autonomous control of the UAV in contact with a fixed object has been achieved. Moreover, the tool is cheap and easy to replace.

The system is still a prototype, and two aspects are planned in future work. Firstly, the optimization of the number of joints and their placement. As mentioned in Section II-B the positioner has 5 DoF, lacking of the one that corresponds to the roll of the drone. This extra degree of freedom has been skipped in order to reduce the weight of the tool and simplify its construction. However, it is considered for later versions. Secondly, the lengths of the bars are fairly chosen to cover a wide workspace and reduce as possible the deadlocks of the tool. Nonetheless, these lengths can be mathematically optimized to fit to specific applications and better avoid critical angles of the joints. Furthermore, accuracy of joints angle measurements can be improved by using more expensive devices, such as high resolution encoders.

Currently, the researchers are working in active placement of the docking tool aided by the second manipulator. Additionally, during the experiments, the arm which holds the docking tool remained at the same position. In future work, the arm will move actively to increase the working volume of the robot.

## ACKNOWLEDGMENT

We thank other members of the *Robotics, Vision and Control Group* for supporting us during this work. This work has been developed in the framework of the EU-funded projects AEROARMS (SI-1439/2015) and HYFLIER (SI-1762/23/2017). We also want to thank the collaboration of Manuel Perez Jimenez, Javier Prada Delgado, Jose Maria Aguilar and the company DroneTools for their assistance on the development of the hexacopter platforms.

## REFERENCES

- [1] S. Montambault, J. Beaudry, K. Toussaint, and N. Pouliot, "On the application of vtol uavs to the inspection of power utility assets," in *2010 1st International Conference on Applied Robotics for the Power Industry*, Oct 2010, pp. 1–7.
- [2] M. Stokkeland, K. Klausen, and T. A. Johansen, "Autonomous visual navigation of unmanned aerial vehicle for wind turbine inspection," in *2015 International Conference on Unmanned Aircraft Systems (ICUAS)*, June 2015, pp. 998–1007.
- [3] P. Addabbo, A. Angrisano, M. L. Bernardi, G. Gagliarde, A. Mennella, M. Nisi, and S. Ullo, "A uav infrared measurement approach for defect detection in photovoltaic plants," in *2017 IEEE International Workshop on Metrology for AeroSpace (MetroAeroSpace)*, June 2017, pp. 345–350.
- [4] M. Orsag, C. Korpela, and P. Oh, "Modeling and control of mm-uav: Mobile manipulating unmanned aerial vehicle," *Journal of Intelligent & Robotic Systems*, vol. 69, no. 1, pp. 227–240, Jan 2013. [Online]. Available: <https://doi.org/10.1007/s10846-012-9723-4>
- [5] V. Lippiello and F. Ruggiero, "Cartesian impedance control of a uav with a robotic arm," *IFAC Proceedings Volumes*, vol. 45, no. 22, pp. 704 – 709, 2012, 10th IFAC Symposium on Robot Control.
- [6] F. Ruggiero, M. A. Trujillo, R. Cano, H. Ascorbe, A. Viguria, C. Perz, V. Lippiello, A. Ollero, and B. Siciliano, "A multilayer control for multirotor uavs equipped with a servo robot arm," in *2015 IEEE International Conference on Robotics and Automation (ICRA)*, May 2015, pp. 4014–4020.
- [7] S. Kim, S. Choi, and H. J. Kim, "Aerial manipulation using a quadrotor with a two dof robotic arm," in *2013 IEEE/RSJ International Conference on Intelligent Robots and Systems*, Nov 2013, pp. 4990–4995.
- [8] C. Korpela, M. Orsag, and P. Oh, "Towards valve turning using a dual-arm aerial manipulator," in *2014 IEEE/RSJ International Conference on Intelligent Robots and Systems*, Sept 2014, pp. 3411–3416.
- [9] A. Suarez, A. E. Jimenez-Cano, V. M. Vega, G. Heredia, A. Rodriguez-Castao, and A. Ollero, "Lightweight and human-size dual arm aerial manipulator," in *2017 International Conference on Unmanned Aircraft Systems (ICUAS)*, June 2017, pp. 1778–1784.
- [10] T. W. Danko, K. P. Chaney, and P. Y. Oh, "A parallel manipulator for mobile manipulating uavs," in *2015 IEEE International Conference on Technologies for Practical Robot Applications (TePRA)*, May 2015, pp. 1–6.
- [11] V. Parra-Vega, A. Sanchez, and C. Izaguirre, "Toward force control of a quadrotor uav in  $se(3)$ ," in *2012 IEEE 51st IEEE Conference on Decision and Control (CDC)*, Dec 2012, pp. 1802–1809.
- [12] T. Bartelds, A. Capra, S. Hamaza, S. Stramigioli, and M. Fumagalli, "Compliant aerial manipulators: Toward a new generation of aerial robotic workers," *IEEE Robotics and Automation Letters*, vol. 1, no. 1, pp. 477–483, Jan 2016.
- [13] R. Mur-Artal and J. D. Tardós, "ORB-SLAM2: an open-source SLAM system for monocular, stereo and RGB-D cameras," vol. 33, no. 5, 2017, pp. 1255–1262.
- [14] M. Labb and F. Michaud, "Online global loop closure detection for large-scale multi-session graph-based slam," 2014.
- [15] J. Zhang and S. Singh, "Loam: Lidar odometry and mapping in real-time," 07 2014.
- [16] L. Meier, P. Tanskanen, F. Fraundorfer, and M. Pollefeys, "Pixhawk: A system for autonomous flight using onboard computer vision," in *2011 IEEE International Conference on Robotics and Automation*, May 2011, pp. 2992–2997.
- [17] L. Meier, D. Honegger, and M. Pollefeys, "Px4: A node-based multithreaded open source robotics framework for deeply embedded platforms," in *2015 IEEE International Conference on Robotics and Automation (ICRA)*, May 2015, pp. 6235–6240.
- [18] S. Thrun, W. Burgard, and D. Fox, *Probabilistic Robotics (Intelligent Robotics and Autonomous Agents)*. The MIT Press, 2005.